COMMUNICATIONS IN COMPUTATIONAL PHYSICS
Vol. **4**, No. 2, pp. 378-404

Commun. Comput. Phys.
August 2008

A New Stable Version of the SPH Method in Lagrangian Coordinates

A. Ferrari, M. Dumbser, E. F. Toro and A. Armanini*

Laboratory of Applied Mathematics, Faculty of Engineering, University of Trento, Trento 38100, Italy.

Received 15 October 2007; Accepted (in revised version) 18 January 2008

Available online 18 March 2008

Abstract. The purpose of this paper is to solve some of the trouble spots of the classical SPH method by proposing an alternative approach. First, we focus on the problem of the stability for two different SPH schemes, one is based on the approach of Vila [25] and another is proposed in this article which mimics the classical 1D Lax-Wendroff scheme. In both approaches the classical SPH artificial viscosity term is removed preserving nevertheless the linear stability of the methods, demonstrated via the von Neumann stability analysis. Moreover, the issue of the consistency for the equations of gas dynamics is analyzed. An alternative approach is proposed that consists of using Godunov-type SPH schemes in Lagrangian coordinates. This not only provides an improvement in accuracy of the numerical solutions, but also assures that the consistency condition on the gradient of the kernel function is satisfied using an equidistant distribution of particles in Lagrangian mass coordinates. Three different Riemann solvers are implemented for the first-order Godunov type SPH schemes in Lagrangian coordinates, namely the Godunov flux based on the exact Riemann solver, the Rusanov flux and a new modified Roe flux, following the work of Munz [17]. Some well-known numerical 1D shock tube test cases [22] are solved, comparing the numerical solutions of the Godunov-type SPH schemes in Lagrangian coordinates with the first-order Godunov finite volume method in Eulerian coordinates and the standard SPH scheme with Monaghan's viscosity term.

AMS subject classifications: 52B10, 65D18, 68U05, 68U07

Key words: SPH, meshfree particle methods, Riemann solvers, gas dynamics in Lagrangian coordinates, Godunov type schemes.

1 Introduction

The Smoothed Particle Hydrodynamics (SPH) method was originally introduced by Lucy [11], Gingold and Monaghan [5]. It is one of the earliest particle methods in compu-

*Corresponding author. *Email addresses:* ferraria@ing.unitn.it (A. Ferrari), dumbserm@ing.unitn.it (M. Dumbser), eleuterio.toro@ing.unitn.it (E. F. Toro), aronne.armanini@ing.unitn.it (A. Armanini)

tational mechanics and it was devised to simulate a wide variety of problems in astrophysics. Like many meshfree methods, the SPH scheme is based on the Lagrangian approach and it is able to handle problems characterized by large deformations, moving discontinuities and critical mesh distortions.

In the SPH scheme, the generic continuum, such as a fluid, is discretized by a finite set of discrete values defined at observation points, the so-called particles. Each point is not fixed on a mesh, but it moves with the velocity of the fluid and the interactions of each other are determined by a local function, the smoothing kernel. This function is the essential feature of the SPH scheme and it assigns the weights of each particles based on the reciprocal positions of the interpolating points.

Different smoothing functions have been used in the SPH method as seen in the literature [9]. The most widely used kernel functions in the SPH simulations are the Gaussian and the cubic $B-$spline of Monaghan and Lattanzio [15]. In spite of the interesting mathematical properties of the Gaussian function, most practical work relies on the monotone splines [1]. In fact, using the splines and consequently a smaller support, one can obtain more accurate numerical solutions and more efficiency, from the computational point of view. Unfortunately, even the choice of a spline function can not assure us that the consistency conditions on the kernel are always satisfied [9], because the accuracy of the numerical solution depends also on the distribution of the observation points inside the compact support. This effect is emphasized near the boundaries, when the kernel support leaves the numerical domain and thus the distribution of the particles is unbalanced, but it can be also significant within the computational domain, when the particles are placed irregularly. To solve this issue, a new approach is proposed, which is based on an uniform distribution of the particles in the Lagrangian mass coordinates.

Moreover, the classical SPH method suffers from several well-known numerical problems, such as particle interpenetration in high Mach number flows [13] or the so-called tensile instability [14]. Generally one deals with these issues using various artificial pressure and viscosity terms as introduced by Monaghan [12] in the motion and thermal energy equations, but it does not solve all the issues. In fact, a von Neumann analysis was carried out by Balsara [1] on the SPH method with Monaghan's artificial viscosity term. Unfortunately, only a small range of ratios of smoothing length to particle distance for a specified choice of kernel function leads to stable continuum behavior. Based on that finding we deduce that none of the currently used SPH kernels represents a particularly good choice using Monaghan's viscosity term [1]. In spite of that, up to this day the viscosity term proposed by Monaghan has been mostly used.

An alternative approach has been recently proposed by Vila [25] and by Moussa and Vila [16], who studied the convergence of SPH using approximate Riemann solvers instead of the artificial viscosity. Moreover, Parshikov *et al.* [18], according to Godunov schemes in the Finite Volume method, use the result of the Riemann problem in the calculation of the numerical flux. Good results have been also obtained by Cha and Whitworth [3], who have applied the Riemann solver of van Leer [23, 24] to isothermal hydrodynamics. A recent improvement of the order of accuracy of SPH comes from Inut-

suka [7] used a rather complex framework in order to obtain second-order of accuracy in one space dimension.

In this work, we start in Section 2.1 with the linear stability and monotonicity analysis of two different SPH methods applied to the linear advection equation. The methods are the first-order Godunov type SPH scheme, following Vila [25], and a new second-order approximation for the SPH method that mimics the classical Lax-Wendroff scheme. The results identify the stability region and amplitude error contours for each numerical scheme. In Section 2.2 we show some numerical results for two computational test problems with periodic boundary conditions, implemented in order to assess the accuracy of the numerical schemes. In Section 3 we propose an alternative SPH approach to solve the equations of gas dynamics. The idea consists of using Godunov type SPH schemes in Lagrangian coordinates based on the work of Munz [17] and Vila [25]. Different Riemann solvers are implemented (in Section 3.2) and are compared against each other solving some well-known test problems (in Section 3.3) in order to verify the accuracy, robustness and performance of the methods.

2 Linear advection equation

In this section we consider the linear one-dimensional advection equation

$$\begin{cases} \dfrac{\partial u}{\partial t}+\dfrac{\partial f}{\partial \xi}=0, \\ f(u)=au, \end{cases} \tag{2.1}$$

where t and ξ denote the time and the spatial variables, $u(t,\xi)$ is the unknown function, $f(u)$ is the flux and a is the advection speed in positive ξ direction, hence we assume $a>0$. We analyze two different formulations of the SPH scheme: a first-order approximation with the exact Riemann solver to evaluate the numerical flux, following Vila [25], and a new second-order approximation that mimics the classical 1D Lax-Wendroff scheme.

2.1 Stability and accuracy analysis

We consider a finite set of N particles, each of constant mass m_j and density ρ_j (with $j=1,\cdots,N$) in the one-dimensional case. Using the SPH scheme, the value of a certain function $f(\xi)$ and its gradient $\nabla f(\xi)$ at the location ξ_i of the i^{th} observation point is estimated as follows

$$f(\xi_i)=f_i=\sum_{j=1}^{N} V_j f_j W_{ij}, \tag{2.2}$$

$$\nabla f(\xi_i)=\left.\frac{\partial f}{\partial \xi}\right|_i=\sum_{j=1}^{N} V_j f_j \frac{\partial W_{ij}}{\partial \xi_j}, \tag{2.3}$$

where V_j is the volume associated with the j^{th} particle and W_{ij} is the smoothing kernel function, centered in the i^{th} point and defined such that:

$$W_{ij}=W_{ji}, \qquad \nabla W_{ij}=-\nabla W_{ji}. \tag{2.4}$$

It depends on the dimensionless variable $q=\left|\xi_j-\xi_i\right|/l$, the ratio of the distance between the particles to the smoothing length l, and converges to the Dirac function $\delta\left(\xi_j-\xi_i\right)$ as $l\to 0$. It determines the weight of each point and a symmetrical compact support. Only the particles inside the support are actually interpolation points with no null weight in (2.2) and (2.3). Applying the expressions (2.2) and (2.3) to a constant function $f(\xi)$, we obtain the consistency conditions to be satisfied by the smoothing kernel function

$$\sum_{j=1}^{N} V_j W_{ij}=1, \qquad \sum_{j=1}^{N} V_j \frac{\partial W_{ij}}{\partial \xi_j}=0, \qquad \forall i=1,\cdots,N. \tag{2.5}$$

In particular, for a uniform distribution of points in one-dimension we have $V_j=\Delta\xi$ for $j=1,\cdots,N$. In this case the consistency condition on the gradient of the kernel in (2.5) becomes

$$\sum_{j=1}^{N} \frac{\partial W_{ij}}{\partial \xi_j}=0, \tag{2.6}$$

and due to the symmetry of the smoothing kernel (2.4) it is satisfied so that no spurious contributions in the evaluation of the flux are added in (2.1) for a constant state $u(t,\xi)$. In general, when the points are moving irregularly, the consistency condition is no longer satisfied exactly. One of the approaches to solve this discrepancy in SPH is the introduction of an adjusting factor in the kernel function and its gradient [10], to give a corrected kernel [20].

Different smoothing functions can be used in the SPH method. In this section, two types of kernel are used:

- the cubic $B-$spline function

$$W^c(q,l)=\frac{1}{l}\begin{cases} 2/3-q^2+q^3/2 & \text{if } 0\le q<1, \\ (2-q)^3/6 & \text{if } 1\le q\le 2, \\ 0 & \text{if } q>2. \end{cases} \tag{2.7}$$

- the truncated Gaussian function

$$W^g(q,l)=\frac{1}{l\sqrt{\pi}}\begin{cases} e^{-q^2} & \text{if } 0\le q\le 3, \\ 0 & \text{if } q>3. \end{cases} \tag{2.8}$$

Applying the standard SPH approximation as in (2.3) at point ξ_i together with explicit forward Euler time stepping to Eq. (2.1) gives

$$u_i^{n+1}=u_i^n-a\ \Delta t\sum_{j=1}^{N} V_j u_j^n \frac{\partial W_{ij}}{\partial \xi}, \tag{2.9}$$

where u_i^{n+1} and u_i^n indicate the values of the unknown function u at time steps $n+1$ and n, respectively.

From (2.9), the standard SPH method can be interpreted as an explicit centered finite difference scheme that is *unconditionally unstable* using explicit Euler time stepping. In order to demonstrate this, we consider the von Neumann method that is based on harmonic analysis assuming the following trial solution

$$u = u(t^n,\xi) = u_0^n \cdot e^{I(\mathrm{K}\,\xi)}, \qquad \mathrm{K} = \frac{\phi}{\Delta\xi}, \tag{2.10}$$

where K is the wave number, ϕ is the phase angle, u_0^n is the amplitude of the harmonic at time t^n and I denotes the imaginary unit with $I^2 = -1$.

The purpose of the analysis is to study the evolution of the amplitude of the harmonic in the time, focusing on the estimate of the modulus of the amplification factor defined as

$$\left\|\hat{A}_f\right\| = \left\| \frac{u_0^{n+1}}{u_0^n} \right\|, \qquad \hat{A}_f = \hat{A}_f\left(C_{cfl},\phi\right), \tag{2.11}$$

where C_{cfl} is the Courant number, defined as $C_{cfl} = a\Delta t/\Delta\xi$. The linear stability region of each scheme is identified by the following condition

$$\left\|\hat{A}_f\right\| \le 1 \qquad \forall C_{cfl}, \forall\phi \in [0;\pi]. \tag{2.12}$$

Applying the von Neumann analysis to (2.9) one obtain

$$\left\| \frac{u_0^{n+1}}{u_0^n} \right\| = \left\| 1 - a\ \Delta t \sum_{j=1}^{N} V_j e^{I\mathrm{K}\left(\xi_j-\xi_i\right)} \frac{\partial W_{ij}}{\partial\xi} \right\|. \tag{2.13}$$

From the smoothed particle approximation (2.3) of the SPH method, we can write

$$\sum_{j=1}^{N} V_j e^{I\mathrm{K}\left(\xi_j-\xi_i\right)} \frac{\partial W_{ij}}{\partial\xi} \cong \alpha \left.\frac{\partial e^{I\mathrm{K}\xi}}{\partial\xi}\right|_i \frac{1}{e^{I\mathrm{K}\xi_i}} + \mathcal{O}\left(\Delta\xi^2\right), \tag{2.14}$$

that is, neglecting the higher order term $\mathcal{O}\left(\Delta\xi^2\right)$

$$\alpha I\mathrm{K} = \alpha I \frac{\phi}{\Delta\xi}, \tag{2.15}$$

where α denotes the error in the approximation (2.3), that is $\alpha = 1$ for the cubic $B-$spline and $\alpha \cong 1$ for the truncated Gaussian function, choosing the smoothing length $l = 2\xi$. It follows that the stability condition (2.12) is never satisfied because

$$\left| 1 - \alpha I\phi \frac{a\ \Delta t}{\Delta\xi} \right| = \sqrt{1+\alpha^2 C_{cfl}^2\phi^2}, \qquad \forall\phi, C_{cfl}. \tag{2.16}$$

Therefore, it is necessary to stabilize the original version of the SPH method (2.9). In general, Monaghan's viscosity term is used. Otherwise we produce a new version of the standard SPH method by introducing higher-order space and time derivatives in (2.9). The resulting new SPH scheme mimics the stable one-dimensional Lax-Wendroff finite difference scheme. It results by applying the Cauchy-Kowalewsky procedure to the linear advection equation (2.1), replacing time derivatives by space derivatives in the Taylor series expansion in time

$$u_i^{n+1} = u_i^n - a\ \Delta t \sum_{j=1}^{N} V_j u_j^n \frac{\partial W_{ij}}{\partial \xi_j} + \frac{1}{2}(a\ \Delta t)^2 \sum_{j=1}^{N} V_j u_j^n \frac{\partial^2 W_{ij}}{\partial \xi_j^2}. \tag{2.17}$$

With this approach, one could also construct higher-order Lax-Wendroff type schemes by considering the higher-order derivatives in time and space.

An alternative upwind version of the SPH scheme has been proposed by Vila [25], Moussa and Vila [16], who introduced the use of Riemann solvers in order to evaluate numerical fluxes between two interacting particles, i^{th} and j^{th}. Their scheme reads as

$$u_i^{n+1} = u_i^n - \Delta t \sum_{j=1}^{N} V_j 2 f_{ij} \frac{\partial W_{i,j}}{\partial \xi_j}, \tag{2.18}$$

where a numerical flux $f_{ij} = f_{ij}(u_i, u_j)$ is introduced. Using the exact Riemann solver for (2.1), the flux f_{ij} is defined as:

$$f_{ij} = a \begin{cases} u_i^n & \text{if } a \cdot (\xi_j - \xi_i) < 0, \\ u_j^n & \text{if } a \cdot (\xi_j - \xi_i) > 0. \end{cases} \tag{2.19}$$

We analyze the stability of the SPH formulations (2.17)-(2.18) by using the von Neumann method (2.10) and (2.12). Since each numerical scheme can be written as:

$$u_i^{n+1} = \sum_{ii=-\alpha_L}^{\alpha_R} c_{ii}^{**} u_{i+ii}^n, \tag{2.20}$$

where the coefficients c_{ii}^{**} and the integers α_L and α_R depend on the scheme, the stability condition for (2.20) reads as:

$$\left\| \hat{A}_f(\mathrm{K}) \right\| = \left\| \sum_{ii=-\alpha_L}^{\alpha_R} c_{ii}^{**} e^{I(\mathrm{K}\Delta\xi \cdot ii)} \right\| \leq 1 \qquad \forall \phi \in [0;\pi]. \tag{2.21}$$

Because of the rather complex analytical expressions arising in (2.21), the modulus of the amplification factor has been evaluated numerically

$$\left\| A_f \right\| = \max_{\phi \in [0;\pi]} \left(\left\| \hat{A}_f(\phi) \right\| \right), \tag{2.22}$$

varying:

- the smoothing length l that determines the kernel support and the integers α_L, α_R;
- the phase angle ϕ in the range $0 \leq \phi \leq \pi$;
- the Courant number $C_{cfl} = a\Delta t/\Delta\xi$ in the range $0 \leq C_{cfl} \leq 10$.

The numerical results have identified a stable region for both formulations: the new second-order Lax-Wendroff type SPH scheme and the first-order scheme with the exact Riemann solver. Fig. 1 represents the stable region related to the choice of the kernel and of the numerical scheme. The top frame shows the results using the cubic $B-$spline for the new Lax-Wendroff type SPH scheme (on the left) and the Godunov SPH method with the exact Riemann solver (on the right). Similarly, the bottom frame shows the stable region obtained with the Gaussian kernel function for both numerical schemes.

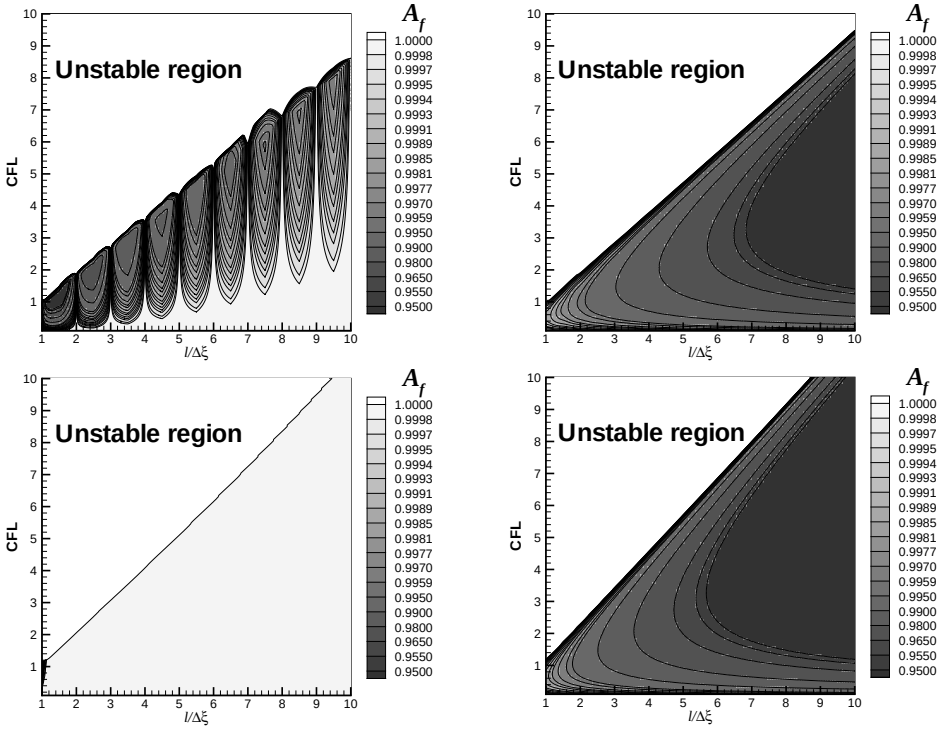

Figure 1: The stability results for two schemes: the Lax-Wendroff type SPH scheme (left) and the SPH scheme with the exact Riemann solver (right). Top: cubic B-spline kernel; Bottom: the Gaussian kernel.

The stable region is very similar in form and area for each graph in Fig. 1, but not the amplitude error contours on the $\left(l/\Delta\xi, C_{cfl}\right)$ plane. The Godunov SPH method with the exact Riemann solver provides regular amplitude error contours using both the cubic $B-$spline and the Gaussian function. Using the Gaussian kernel, the new Lax-Wendroff type SPH approach shows its dispersive nature (i.e., $\left\|A_f\right\|$ is very close to one) and, especially with the cubic $B-$spline, it is very sensitive to small variations of the ratio between the smoothing length l and the mesh size $\Delta\xi$ or of the Courant number C_{cfl}.

With the Gaussian kernel function, both numerical schemes give more stable results, but unfortunately it has a larger support than that of the cubic $B-$spline (2.7) so it is less accurate.

Moreover, for both numerical schemes the limit which assures the stability of the discrete solutions has the form

$$\left(C_{cfl}\right)_{\text{stability}} \leq \beta \frac{l}{\Delta\xi}. \tag{2.23}$$

where β depends on the numerical scheme and on the kernel function, as we can note from the stability results in Fig. 1.

At this point, the monotonicity of both SPH schemes is analyzed. Using the expression (2.20), a sufficient condition for the scheme to remain monotone is that all coefficients c_{ii}^{**} are positive or zero:

$$c_{ii}^{**} \geq 0, \qquad \forall ii \in [-\alpha_L;\alpha_R], \tag{2.24}$$

according to Toro [22]. From the analysis of the monotonicity, the Lax-Wendroff type SPH scheme is not monotone, similar to the second-order Lax-Wendroff finite difference method. For the Godunov type SPH scheme (2.18) the monotonicity condition results

$$-\frac{\partial W_{i,i+ii}}{\partial \xi_{i+ii}} \geq 0, \qquad \text{for} -\alpha_L \leq ii < 0. \tag{2.25}$$

According to the definition of the kernel (2.4), the expression (2.25) is always satisfied for the cubic $B-$spline (2.7) and the Gaussian function (2.8). Special care is required for the analysis of the sign for the c_0^{**} coefficient

$$c_0^{**} = 1 - \Delta t\,(2a) \sum_{ii=1}^{\alpha_R} V_{i+ii} \frac{\partial W_{i,i+ii}}{\partial \xi_{i+ii}} \geq 0. \tag{2.26}$$

Regarding a uniform distribution of particles and using a constant smoothing length $l = m\Delta\xi$, the expression (2.26) leads to

$$c_0^{**} = 1 - C_{cfl}\,(\Delta\xi)^2 2 \sum_{ii=1}^{m\tilde{q}} \frac{\partial W_{i,i+ii}}{\partial \xi_{i+ii}} \geq 0, \tag{2.27}$$

where the integer $\tilde{q}$ depends on the type of the kernel. It can be verified that $\tilde{q} = 3$ for the Gaussian function, $\tilde{q} = 2$ for the cubic $B-$spline, according to (2.8) and (2.7).

When the conditions (2.21) and (2.27) are satisfied, both the stability and the monotonicity of the Godunov SPH scheme are assured. In Table 1 the maximum admissible values of the Courant number C_{cfl} are reported, related to the ratio $l/\Delta\xi$. Note that the monotonicity condition (2.27) is more restrictive than the stability condition.

Table 1: Stability and monotonicity conditions for the Courant number.

		Stability limit					
	$l/\Delta\xi$	1.	2.	3.	4.	5.	10.
Gaussian kernel	C_{cfl}	1.20	2.30	3.40	4.55	5.70	11.50
Cubic $B-$spline	C_{cfl}	1.00	1.90	2.85	3.75	4.70	9.45
		Monotonicity limit					
	$l/\Delta\xi$	1.	2.	3.	4.	5.	10.
Gaussian kernel	C_{cfl}	1.09	1.85	2.70	3.58	4.46	8.87
Cubic $B-$spline	C_{cfl}	1.00	1.60	2.31	3.05	3.79	7.51

2.2 Computational tests

Two computational test cases are proposed for the linear advection equation (2.1) on the computational domain $\Omega=[0,1]$ with periodic boundary conditions. We use 200 particles to discretize the computational domain. In the first case, data consists of two constant states, separated by a discontinuity at a position $\xi=0.5$

$$u_0(\xi)=\begin{cases} 1.0 & \text{if } \xi\leq 0.5, \\ 0.25 & \text{if } \xi>0.5. \end{cases} \tag{2.28}$$

A second discontinuity is on the boundaries due to the periodic boundary conditions.

In the second test the initial condition corresponds to a smooth Gaussian distribution

$$u_0(\xi)=\frac{1}{4}+e^{-8\left[4(\xi-\frac{1}{2})\right]^2}. \tag{2.29}$$

The numerical solutions have been obtained using the Godunov SPH scheme with the exact Riemann solver and the Lax-Wendroff type SPH scheme. Fig. 2 shows the numerical results obtained with both schemes after one and after five periods of advection, compared to the exact solution. The exact solution in both cases consists of a mere translation of the initial condition with constant velocity $a=1$ in (2.1). The numerical solution of the Godunov SPH scheme with the exact Riemann solver is monotone, as demonstrated above, but very diffusive. This effect increases in time, especially in the second test case with a smooth initial condition where the amplitude of the Gaussian distribution decreases considerably after five periods. On the other hand, the numerical solution obtained by the new SPH scheme with the Lax-Wendroff-type approach shows a dispersive and non-monotone nature of the scheme, although at least stable. In the first test large oscillations have been produced in the vicinity of the discontinuities. In the second case the scheme is less diffusive than the Godunov type SPH scheme, but it yields a phase error, more evident after five periods.

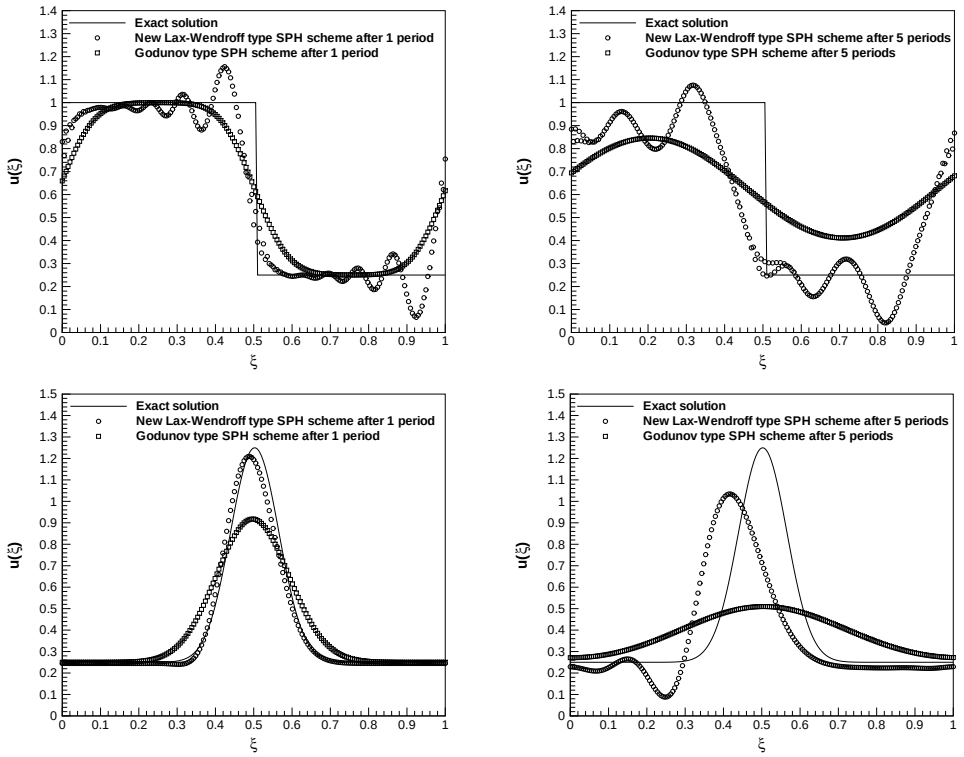

Figure 2: The Godunov SPH scheme (circle) and the Lax-Wendroff type SPH scheme (square) applied to tests (2.28) on the top and (2.29) on the bottom. Numerical (symbol) and exact (line) solutions are compared at output time 1 period (on the left) and 5 periods (on the right).

3 Euler equations in Lagrangian coordinates

After the stability analysis, we consider the problem of the consistency conditions. As seen in the literature [9] and [20], the accuracy of the SPH method depends on the number and on the distribution of the observation points inside the kernel support. In particular, the consistency condition on the gradient of the kernel is always satisfied when the particles are uniformly placed, as deduced in Section 2.1.

Following these remarks, we propose a new approach, which is able to reproduce exactly linear data through an SPH interpolation and provides also an improvement in the accuracy. The new idea consists of using Godunov-type SPH schemes in Lagrangian coordinates. In this way, it is possible to distinguish the computational space (ξ,t) in Lagrangian coordinates, from the physical domain (x,t) in Eulerian coordinates. The points are fixed and uniformly spaced during the whole time evolution in the numerical domain (ξ,t) and only in the physical domain (x,t) the particles are moving. Therefore, all the numerical estimations are computed over the uniformly distributed points in Lagrangian coordinates. This provides some advantages. First, the consistency condition on

the gradient of the kernel is always satisfied during the whole time evolution. Moreover, following the truncation error analysis developed by Quinlan *et al.* [19] for the approximation of spatial derivatives in SPH, for uniformly spaced particles the total error is the sum of a second-order error in l (smoothing error) and an order $(\beta+2)$ error in $\Delta x/l$ (due to discretization of the smoothing integral), with $\beta=2$ for the cubic B-spline kernel.

In the following, we focus on the equations of gas dynamics in Section 3.1, explaining the SPH schemes in Section 3.2 and presenting the numerical results in Section 3.3.

3.1 Governing equations

We consider the Euler equations for an ideal gas in Cartesian coordinates (x,t) in one dimension:

$$\frac{\partial \tilde{\mathbf{U}}}{\partial t}+\frac{\partial \tilde{\mathbf{F}}}{\partial x}=0, \tag{3.1}$$

where $\tilde{\mathbf{U}}$ is the vector of the conserved variables and $\tilde{\mathbf{F}}$ is the flux:

$$\tilde{\mathbf{U}}=\begin{pmatrix} \rho & \rho v & \rho E \end{pmatrix}, \qquad \tilde{\mathbf{F}}=\begin{pmatrix} \rho v \\ \rho v^2+p \\ v(\rho E+p) \end{pmatrix}. \tag{3.2}$$

Here v is the velocity, p denotes the pressure, ρ is the density and E the specific total energy, defined as:

$$E=\frac{1}{2}v^2+\frac{1}{\gamma-1}\frac{p}{\rho}, \tag{3.3}$$

where γ is the ratio of specific heats. The system of equations (3.1) is hyperbolic and in conservation form. According to Courant and Friedrichs [4], it is possible to transform the system (3.1) to Lagrangian coordinates (ξ,t) so that the changing position of each point is given by a function $x(\xi,t)$. A natural choice for ξ is based on the law of the conservation of mass:

$$\xi=\int_{x(0,t)}^{x(\xi,t)}\rho(s,t)\,ds. \tag{3.4}$$

Differentiating with respect to ξ one obtains

$$dx=v\,dt+\frac{1}{\rho}d\xi. \tag{3.5}$$

Then, the conservation laws (3.1) take the form:

$$\frac{\partial \mathbf{U}}{\partial t}+\frac{\partial \mathbf{F}}{\partial \xi}=0, \tag{3.6}$$

where $\mathbf{U}$ is the vector of the conserved variables and $\mathbf{F}$ is the flux, both in Lagrangian coordinates:

$$\mathbf{U}=\begin{pmatrix} \tilde{V} \\ v \\ E \end{pmatrix}, \qquad \mathbf{F}=\begin{pmatrix} -v \\ p \\ vp \end{pmatrix}. \tag{3.7}$$

Here $\tilde{V}$ denotes the specific volume

$$\tilde{V}=\frac{1}{\rho}. \tag{3.8}$$

The system (3.7) is in conservation form. Solutions of (3.1) are equivalent to solutions of (3.7), see Wagner [26]. Note that using the transformation (3.5) it is possible to pass from Eulerian coordinates (x,t) to mass coordinates (ξ,t), understanding the Lagrangian space as computational domain, where the position of the interpolating elements is fixed. Then, the new approach in Lagrangian coordinates allows us to distribute uniformly the points in mass coordinates (ξ,t) and subsequently to assign the properties $W=[\rho,v,p]$ to each particle, taking care to reproduce the physical domain. In this way, the consistency condition on the gradient of the kernel (2.5) is satisfied (see Section 2.1) without an adaptive kernel estimation, very expensive from the computational point of view.

3.2 Numerical schemes

After this brief summary on the Euler equations in Lagrangian coordinates, we now consider the discretization of system (3.7) by the Godunov-type SPH scheme. According to the approximation implemented for the linear advection equation (2.18), the discretization consists of

$$\mathbf{U}_i^{n+1}=\mathbf{U}_i^n-2\Delta t\sum_j^N V_j\mathbf{F}_{ij}^n\frac{\partial W_{ij}}{\partial\xi_j}, \tag{3.9}$$

where $\mathbf{F}_{ij}^n$ is the vector of numerical fluxes evaluated using the solution of the Riemann problem between the states $\mathbf{U}_i^n$, $\mathbf{U}_j^n$ and $V_j=\Delta\xi$ in Lagrangian coordinates.

Many different Riemann solvers are available. For an overview see [22]. In this paper, we use the following fluxes:

- the Godunov flux based on the solution of the exact Riemann solver in Lagrangian coordinates;
- the Rusanov flux in Lagrangian coordinates, corresponding to

$$\begin{cases} \mathbf{F}_{ij}^n=\frac{1}{2}\left(\mathbf{F}_i^n+\mathbf{F}_j^n\right)-\frac{1}{2}C_{ij}\left(\mathbf{U}_j^n-\mathbf{U}_i^n\right), \\ C_{ij}=\max\left(C_i^n,C_j^n\right), \end{cases} \tag{3.10}$$

  where C_i^n denotes the sound speed in Lagrangian coordinates defined at the location i^{th} and time t^n

$$(C_i^n)^2=\gamma\rho_i^n p_i^n. \tag{3.11}$$

- a modified Roe flux in Lagrangian coordinates, defined as follows

$$\mathbf{F}_{ij}^n=\frac{1}{2}\left(\mathbf{F}_i^n+\mathbf{F}_j^n\right)-\frac{1}{2}\tilde{R}_{ij}\left|\tilde{\Lambda}_{ij}\right|\tilde{R}_{ij}^{-1}\left(\mathbf{U}_j^n-\mathbf{U}_i^n\right), \tag{3.12}$$

where $\tilde{\Lambda}_{ij}=diag(\tilde{\lambda}_{ij}^{(1)},\tilde{\lambda}_{ij}^{(2)},\tilde{\lambda}_{ij}^{(3)})$ is the diagonal matrix of the eigenvalues and $\tilde{R}$ is the corresponding matrix of right eigenvectors of the Roe matrix. The flux (3.12) consists of a modification of the scheme proposed by Munz [17], where the eigenvalues of the Roe matrix are:

$$\tilde{\lambda}_{ij}^{(1)}=-\tilde{C}_{ij},\qquad \tilde{\lambda}_{ij}^{(2)}=0,\qquad \tilde{\lambda}_{ij}^{(3)}=+\tilde{C}_{ij}. \tag{3.13}$$

Here $\tilde{C}_{ij}$ is the mean value of the Lagrangian sound velocity

$$\tilde{C}_{ij}^2=\gamma\tilde{\rho}_{ij}\tilde{p}_{ij},\qquad \tilde{\rho}_{ij}=\frac{\rho_i^n+\rho_j^n}{2},\qquad \tilde{p}_{ij}=\frac{p_i^n+p_j^n}{2}. \tag{3.14}$$

Note that due to (3.13) there is *no numerical viscosity* in the Roe flux for the computation of the contact wave. This produces well-known spurious oscillations in the contact wave when solving the Euler equations in Lagrangian coordinates [17]. The phenomenon is not present in Eulerian coordinates. To avoid this, we therefore add a small amount of numerical viscosity for the contact wave by modifying the second eigenvalue $\tilde{\lambda}_2$

$$\tilde{\lambda}_2=\tilde{\alpha}\cdot\max\left(|v_i^n|,|v_j^n|\right), \tag{3.15}$$

where $\tilde{\alpha}$ is a parameter in the range $0\leq\tilde{\alpha}\leq 1$. Note that $\tilde{\alpha}=0$ reproduces the original Roe flux of Munz and $\tilde{\alpha}=1$ leads to a numerical viscosity, equivalent to the amount of numerical viscosity introduced by the Roe scheme in *Eulerian coordinates*.

In the following section, the results of some numerical test cases are presented in comparison with each other and a classical SPH method, reported in the literature by Sigalotti *et al*. [21].

3.3 Numerical results

We have selected four test problems according to [22] for the one-dimensional, time dependent Euler equations for ideal gases with a ratio of specific heats equal to $\gamma=1.4$. The initial conditions are summarized in Table 2. They consist of two constant states $W_L=[\rho_L,v_L,p_L]^T$ on the left and $W_R=[\rho_R,v_R,p_R]^T$ on the right, separated by a discontinuity at a position $x=x_0$. The spatial domain $\Omega=[0,1]$ is discretized by $N=100$ observation points for all test problems. Transmissive boundary conditions have been implemented. The Courant number coefficient depends on the numerical scheme used. Five different schemes have been applied and compared to the exact solution. To have numerical reference solutions, we have implemented the first-order Godunov finite volume (FV) method in conjunction with the exact Riemann solver in Eulerian coordinates (x,t) and the standard SPH method following the work of Sigalotti *et al.* [21], who used the classical approach of the SPH scheme with Monaghan's viscosity term and in addition, an adaptive kernel estimation. Moreover, the Godunov-type SPH schemes in Lagrangian

Table 2: Initial conditions for the numerical test problems.

test	ρ_L	v_L	p_L	ρ_R	v_R	p_R	x_0	T_{end}
1	1.0	0.75	1.0	0.125	0.0	0.1	0.3	0.2
2	1.0	-2.0	0.4	1.0	2.0	0.4	0.5	0.15
3	1.0	0.0	1000.0	1.0	0.0	0.01	0.5	0.012
4	5.99924	19.5975	460.894	5.99242	-6.19633	46.095	0.4	0.035

coordinates (ξ,t) have been implemented with $l/\Delta\xi = 2$. Subsequently the numerical results have been translated into physical coordinates (x,t) according to (3.5), as follows

$$x_i^{n+1} = x_i^n + v_i^n \Delta t + a_i^{n+\frac{1}{2}} \frac{\Delta t^2}{2}, \qquad a_i^{n+\frac{1}{2}} = \frac{1}{\Delta t}\left(v_i^{n+1} - v_i^n\right). \tag{3.16}$$

Three numerical fluxes have been applied, namely the Godunov flux based on the exact Riemann solver in Lagrangian coordinates, the Rusanov flux and the modified Roe flux, see Section 3.2.

Test 1 [22] is a modification of the well-known Sod test problem and it consists of a left rarefaction with a sonic point, an intermediate contact and a right moving shock. The results for test 1 are shown in Figs. 3-7. Unlike the standard SPH scheme, the Godunov-type SPH methods in Lagrangian coordinates approximate the rarefaction wave reasonably well. They produce no discontinuity, the so-called *entropy glitch*, within the rarefaction, typical error of the first-order finite volume (FV) method. The contact discontinuity, seen in the density and internal energy plots, is in general much more difficult to resolve accurately in Eulerian coordinates than shock waves [22] and this is evident in the results of the first-order FV scheme. The numerical resolution of the contact wave is instead reconstructed more accurately than the shock applying the Godunov-type SPH scheme, which is due to the use of Lagrangian coordinates. In particular, the SPH scheme with the Godunov flux computes very well the position of the contact wave, but well-known spurious oscillations near the discontinuity appear. A better resolution for the contact wave is obtained using the modified Roe flux, see Section 3.2. The classical SPH method seems to be not perfectly conservative and large oscillations are visible at the contact wave in the solution profiles for velocity and pressure. The numerical results of a similar test case have been published in the paper of Sigalotti *et al.* [21] and have been computed using *3000* particles in a computational domain $[0,1.2]$, while in this paper the number of points is only *100* in a computational domain $[0,1]$.

Test 2 is useful for assessing the performance of numerical methods for low density flow [22] and its solution corresponds to two strong rarefactions and a stationary contact discontinuity. Figs. 8-12 shows the profiles of the numerical solutions. All the numerical schemes based on the Lagrangian Godunov-type SPH approach compute a quite satisfactory profile for the density, pressure and velocity, but the resolution for internal energy is really inaccurate. The lack of precision may be due to two issues. First, the interpolation points, moving in physical space for the SPH approach, leave the domain because of the

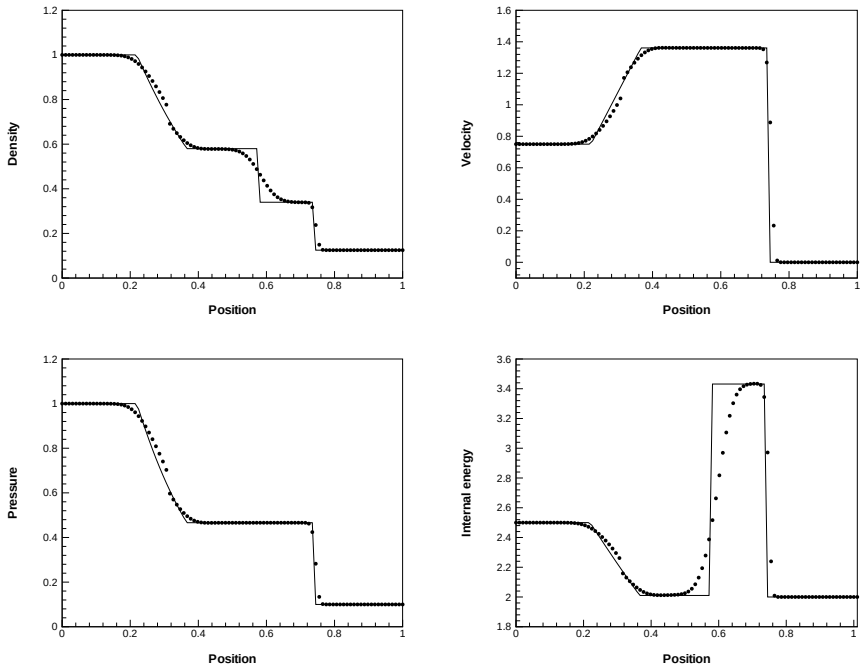

Figure 3: First-order Godunov finite volume scheme applied to test 1. Numerical (symbol) and exact (line) solutions are compared at the output time 0.2 units.

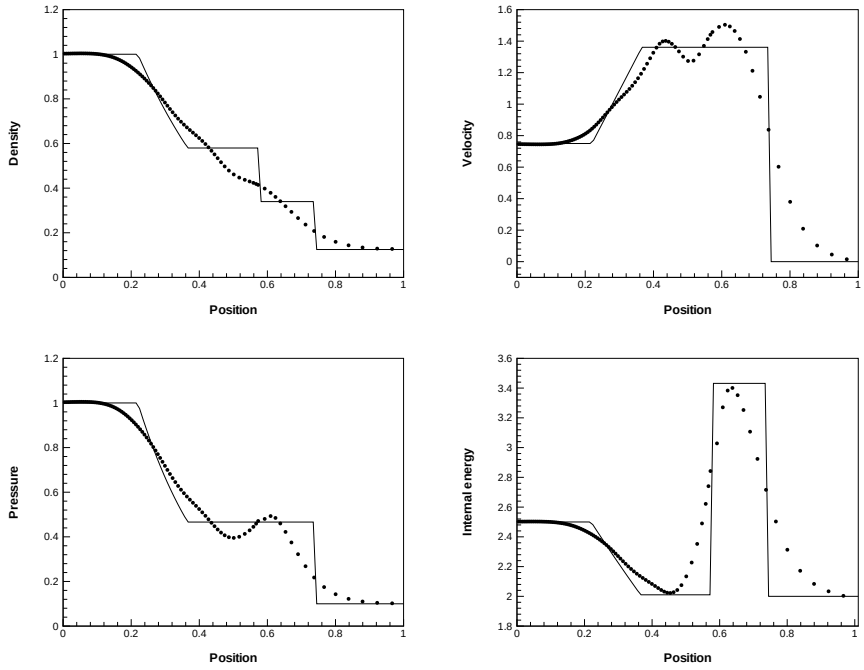

Figure 4: The standard SPH scheme with the adaptive kernel estimation [21] applied to test 1. Numerical (symbol) and exact (line) solutions are compared at the output time 0.2 units.

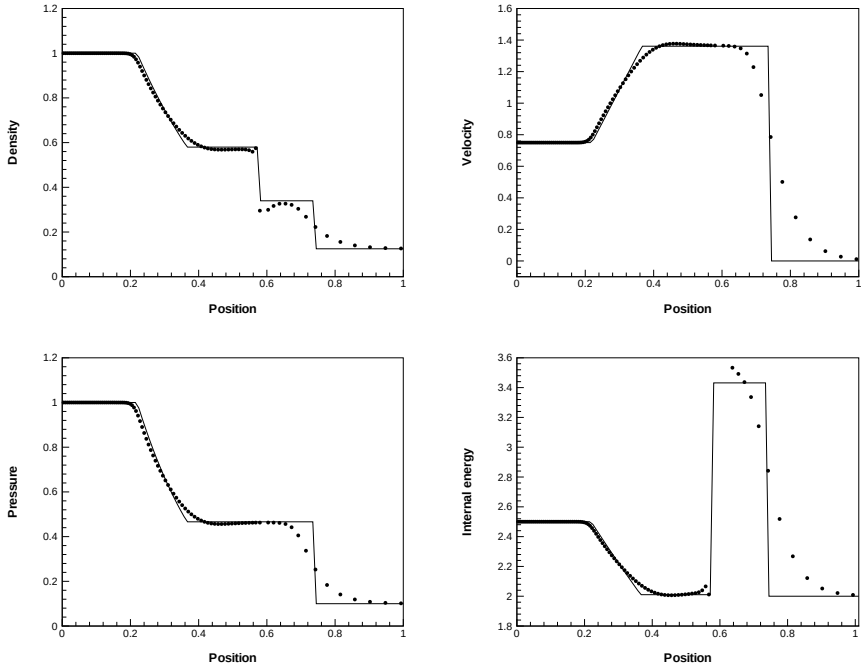

Figure 5: The Godunov-type SPH scheme with the exact Riemann solver applied to test 1. Numerical (symbol) and exact (line) solutions are compared at the output time 0.2 units.

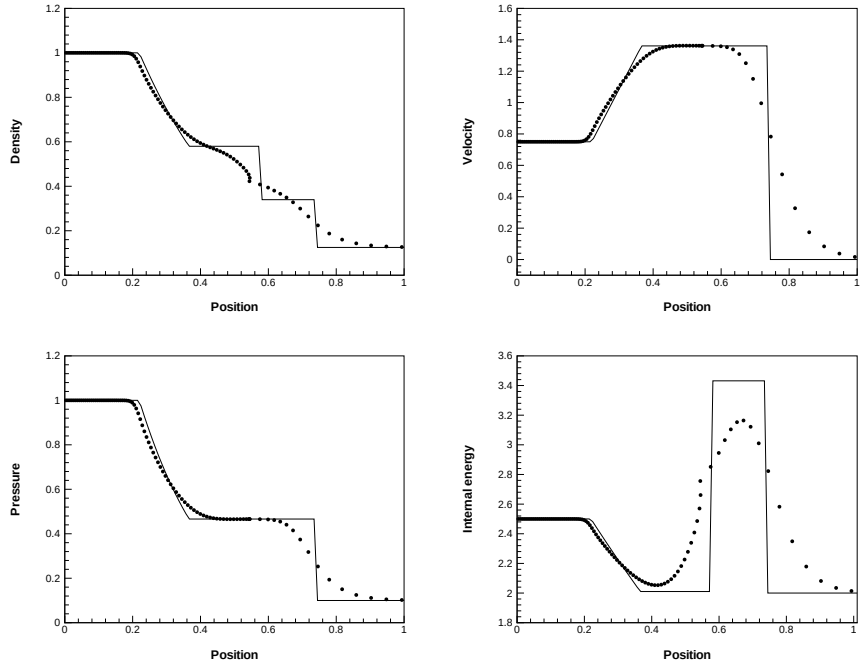

Figure 6: The Godunov-type SPH scheme with the Rusanov flux applied to test 1. Numerical (symbol) and exact (line) solutions are compared at the output time 0.2 units.

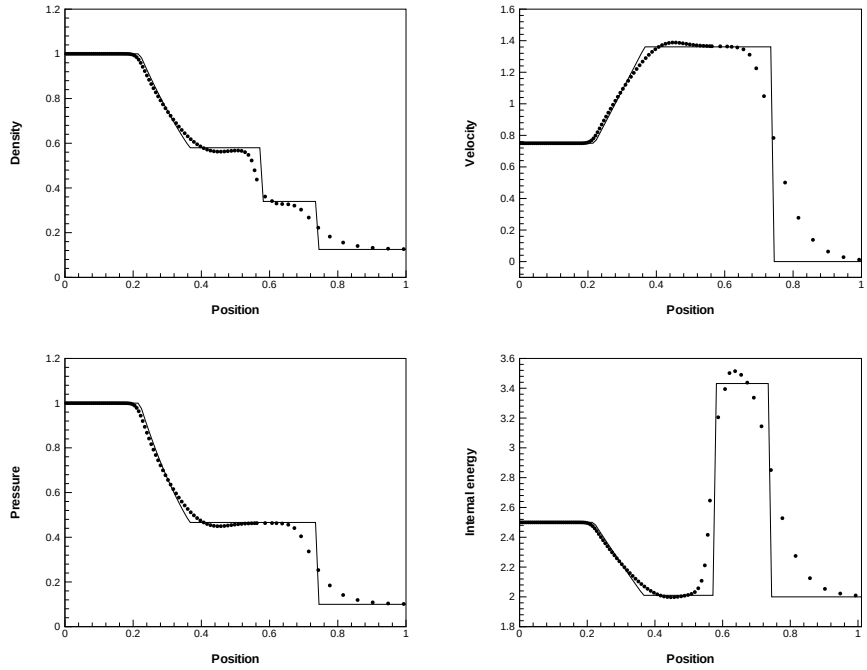

Figure 7: The Godunov-type SPH scheme with the modified Roe flux applied to test 1. Numerical (symbol) and exact (line) solutions are compared at the output time 0.2 units.

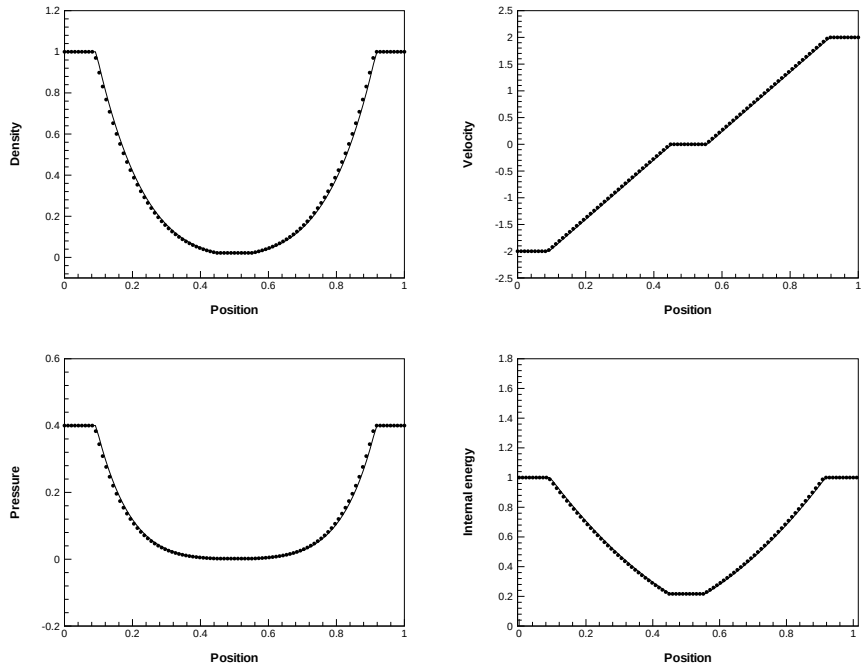

Figure 8: First-order Godunov finite volume scheme applied to test 2. Numerical (symbol) and exact (line) solutions are compared at the output time 0.15 units.

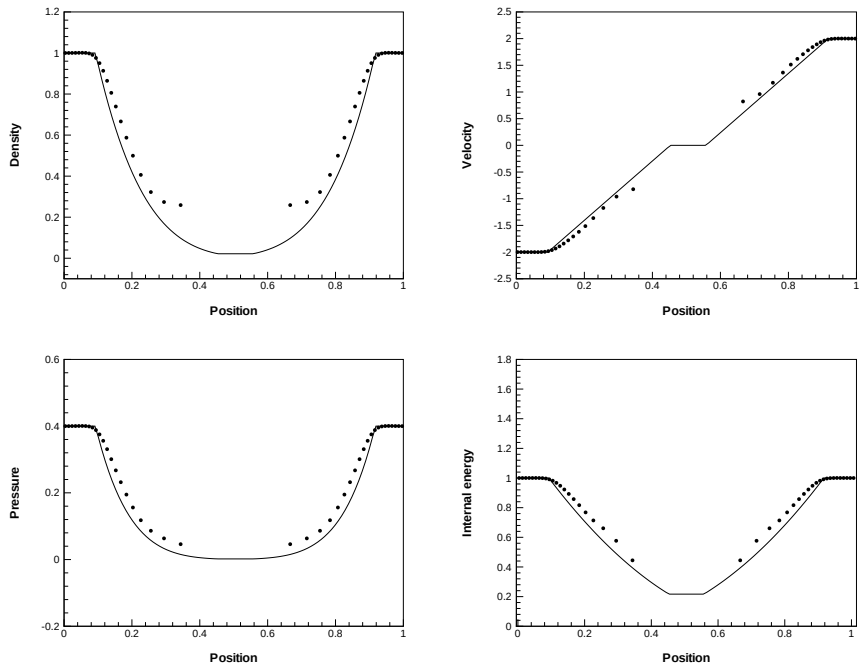

Figure 9: The standard SPH scheme with the adaptive kernel estimation [21] applied to test 2. Numerical (symbol) and exact (line) solutions are plotted at the output time 0.15 units.

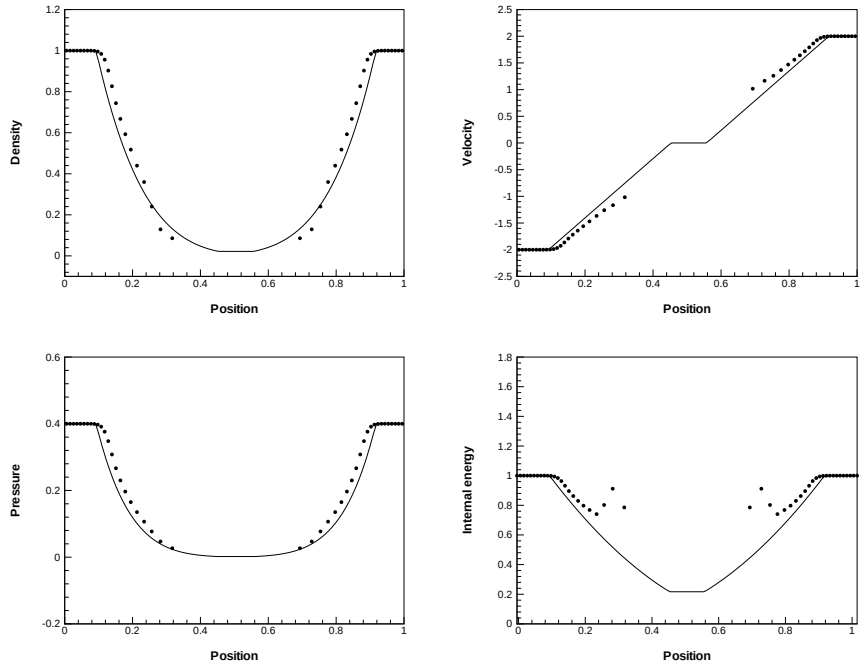

Figure 10: The Godunov-type SPH scheme with the exact Riemann solver applied to test 2. Numerical (symbol) and exact (line) solutions are compared at the time 0.15 units.

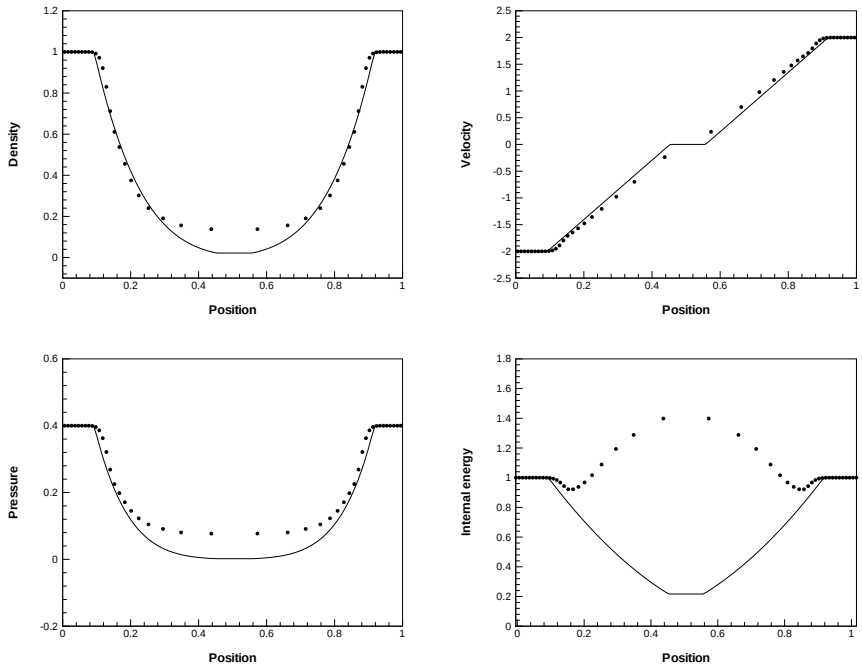

Figure 11: The Godunov-type SPH scheme with the Rusanov flux applied to test 2. Numerical (symbol) and exact (line) solutions are compared at the time 0.15 units.

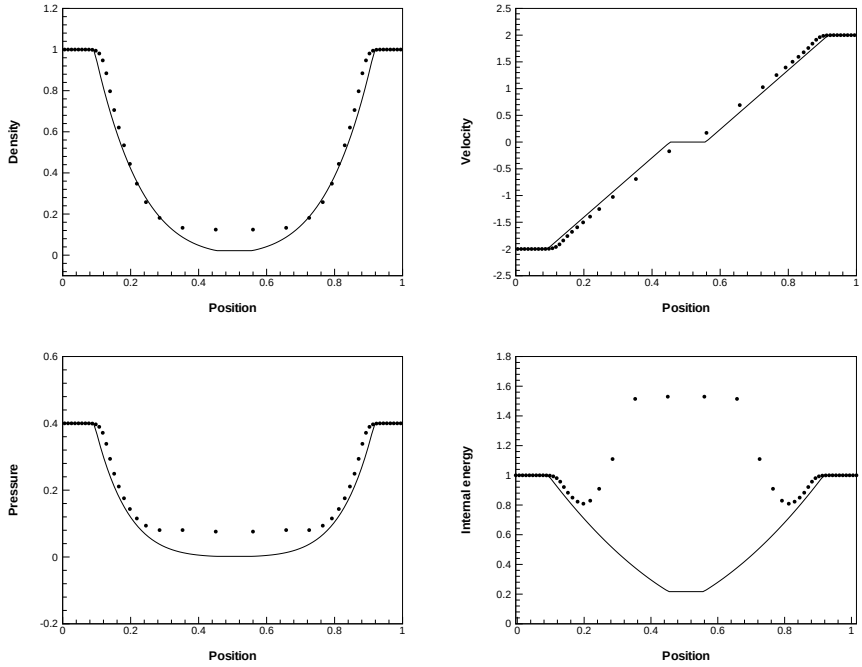

Figure 12: The Godunov-type SPH scheme with the modified Roe flux applied to test 2. Numerical (symbol) and exact (line) solutions are compared at the output time 0.15 units.

velocity field. In this way, the solution profiles in the star region is resolved only with very few points. Moreover, the specific internal energy is computed from the density and the pressure (3.3). In test 2 both density and pressure are close to zero and thus small errors will be exaggerated by their ratio [22].

Test 3 is a very severe problem, the solution of which consists of a left rarefaction, a contact and a rigid shock [22]. The results are plotted in Figs. 13-16. Unfortunately, for test 3, the standard SPH scheme fails using 100 interpolation points. The first-order FV method and the Godunov-type SPH scheme approximate satisfactory well the rarefaction wave for the density, but both produce an overshoot near the tail for the velocity profile. However, this error is smaller for the Godunov-type SPH method. The contact discontinuity and the shock are more accurately solved by the Lagrangian Godunov-type SPH method than by the first-order FV method. In fact, the solution profiles computed by the first-order FV method show a large amount of numerical diffusion. Some differences in correspondence of the contact wave are evident using the three numerical fluxes in the Godunov-type SPH scheme. The Rusanov flux produces a very diffusive solution, the Godunov flux with exact Riemann solver determines spurious oscillations and the modified Roe flux follows accurately the exact solution.

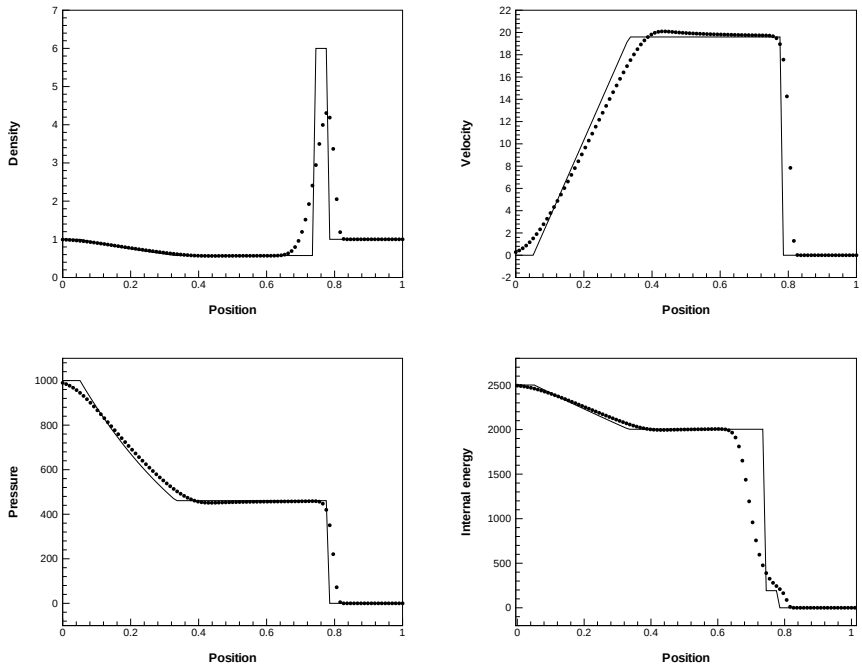

Figure 13: First-order Godunov finite volume scheme applied to test 3. Numerical (symbol) and exact (line) solutions are compared at the output time 0.012 units.

Test case 4 contains three strong discontinuities traveling to the right [22]. The numerical solutions are plotted in Figs. 17-21. As for test 1, the shock waves are more accurate using the first-order FV method, while the contact discontinuity is smeared. The SPH

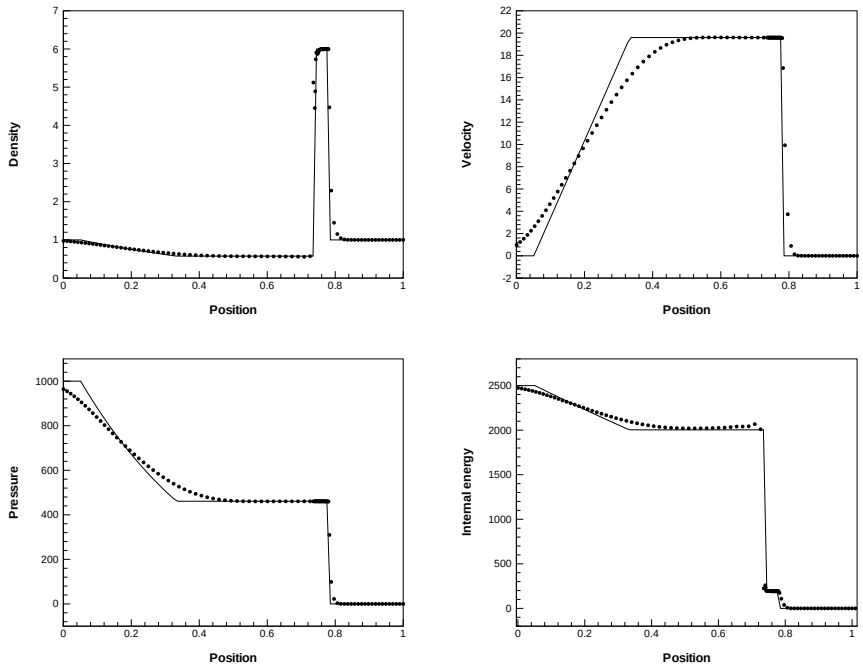

Figure 14: The Godunov-type SPH scheme with the exact Riemann solver applied to test 3. Numerical (symbol) and exact (line) solutions are compared at the time 0.012 units.

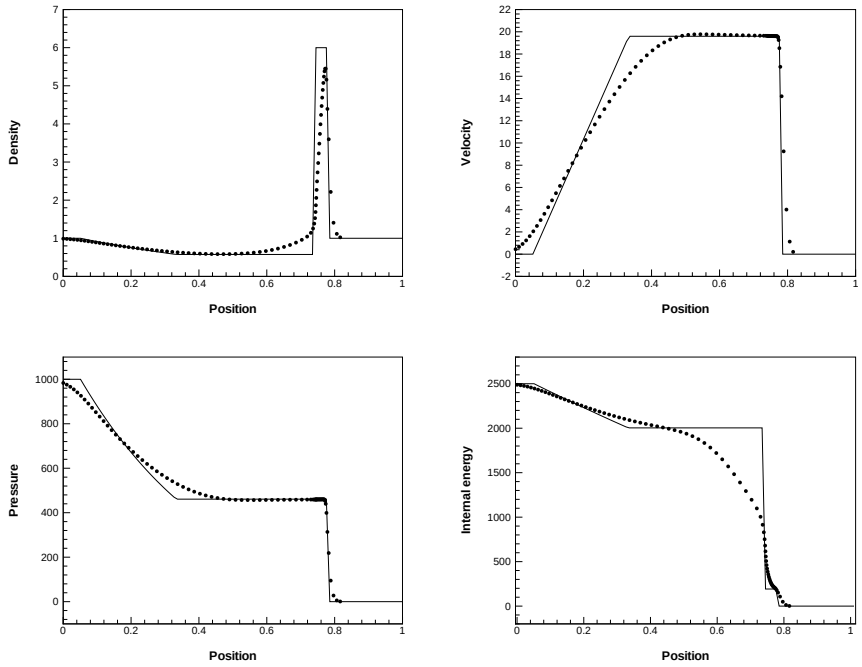

Figure 15: The Godunov-type SPH scheme with the Rusanov flux applied to test 3. Numerical (symbol) and exact (line) solutions are compared at the time 0.012 units.

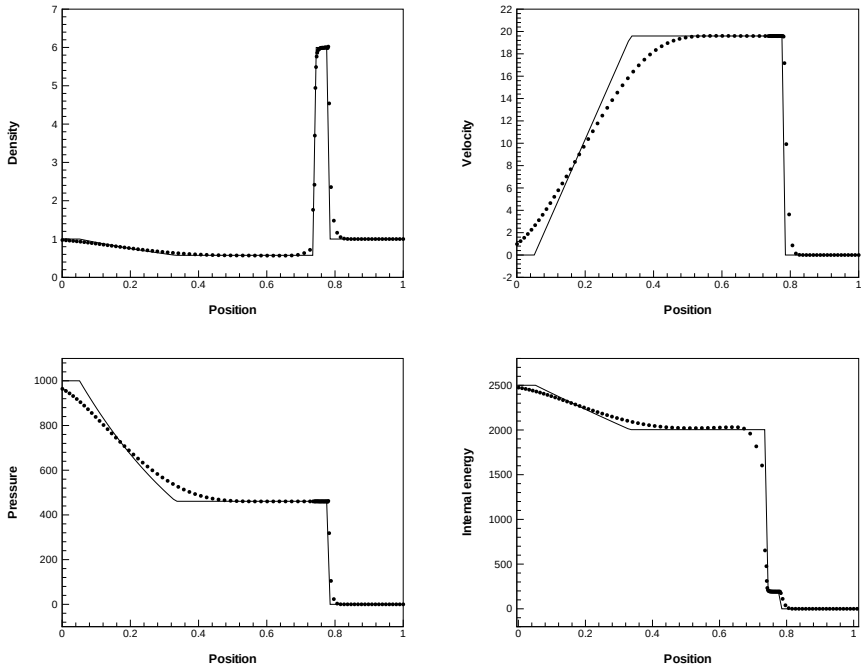

Figure 16: The Godunov-type SPH scheme with the modified Roe flux applied to test 3. Numerical (symbol) and exact (line) solutions are compared at the output time 0.012 units.

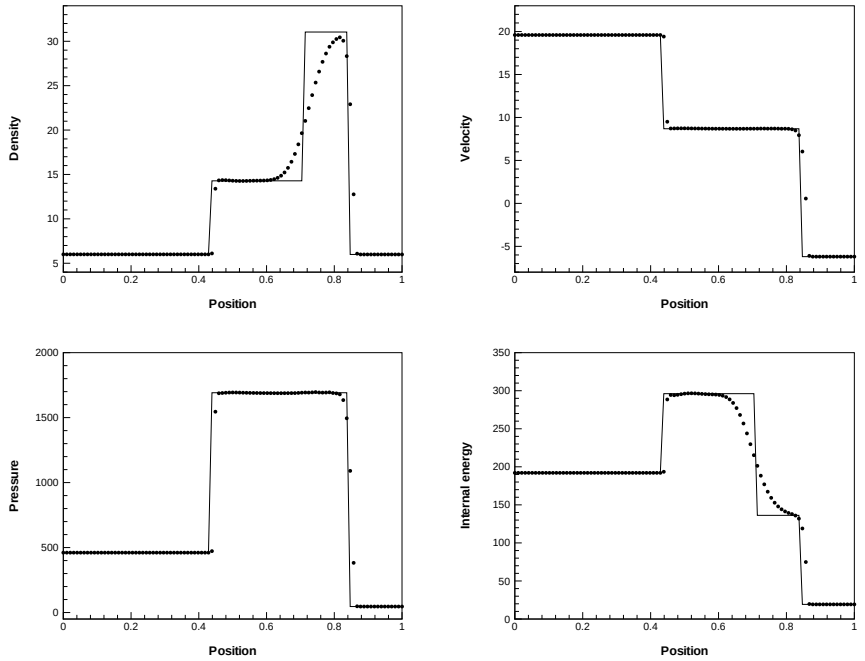

Figure 17: First-order Godunov finite volume scheme applied to test 4. Numerical (symbol) and exact (line) solutions are compared at the output time 0.035 units.

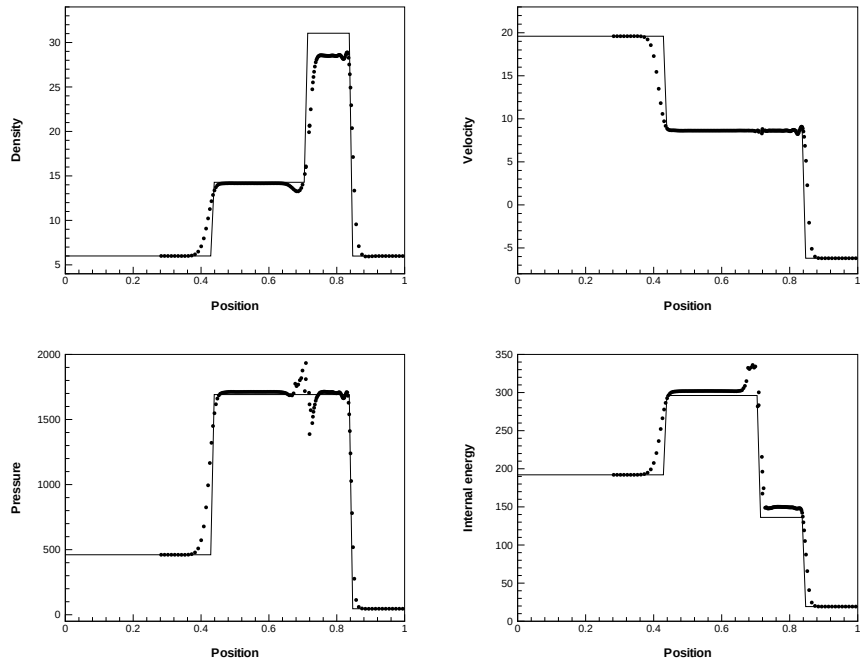

Figure 18: The standard SPH scheme with the adaptive kernel estimation [21] applied to test 4. Numerical (symbol) and exact (line) solutions are plotted at the output time 0.035 units.

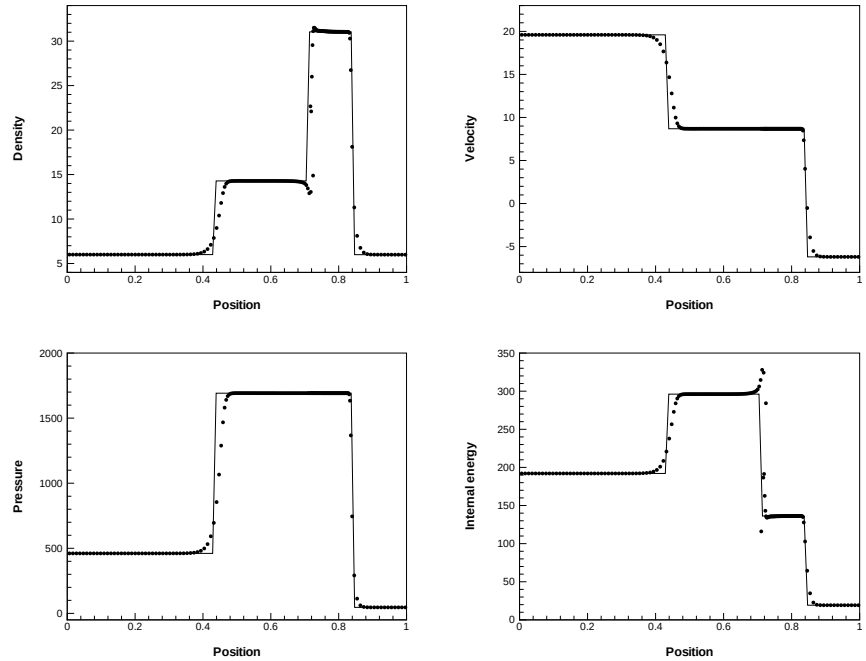

Figure 19: The Godunov-type SPH scheme with the exact Riemann solver applied to test 4. Numerical (symbol) and exact (line) solutions are compared at the time 0.035 units.

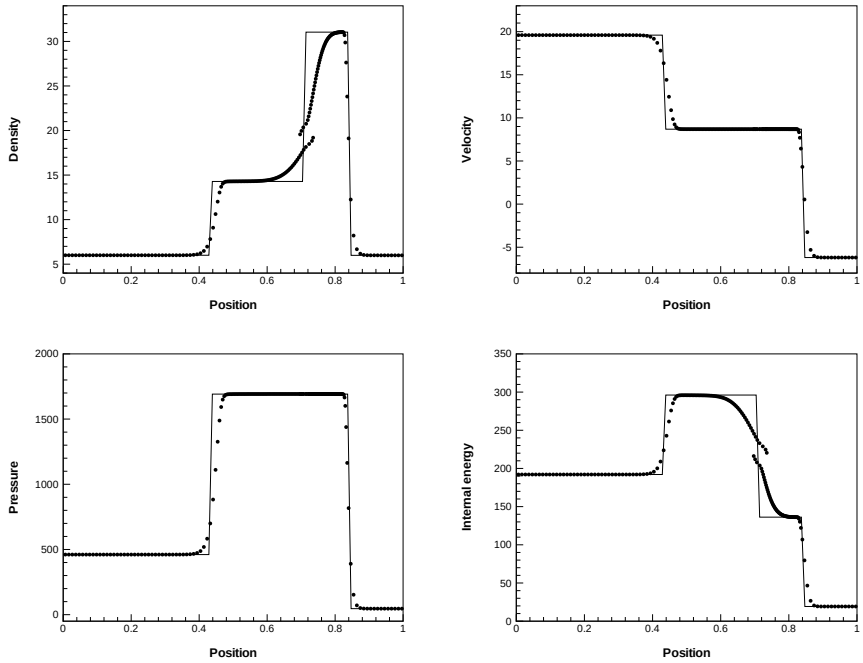

Figure 20: The Godunov-type SPH scheme with the Rusanov flux applied to test 4. Numerical (symbol) and exact (line) solutions are compared at the time 0.035 units.

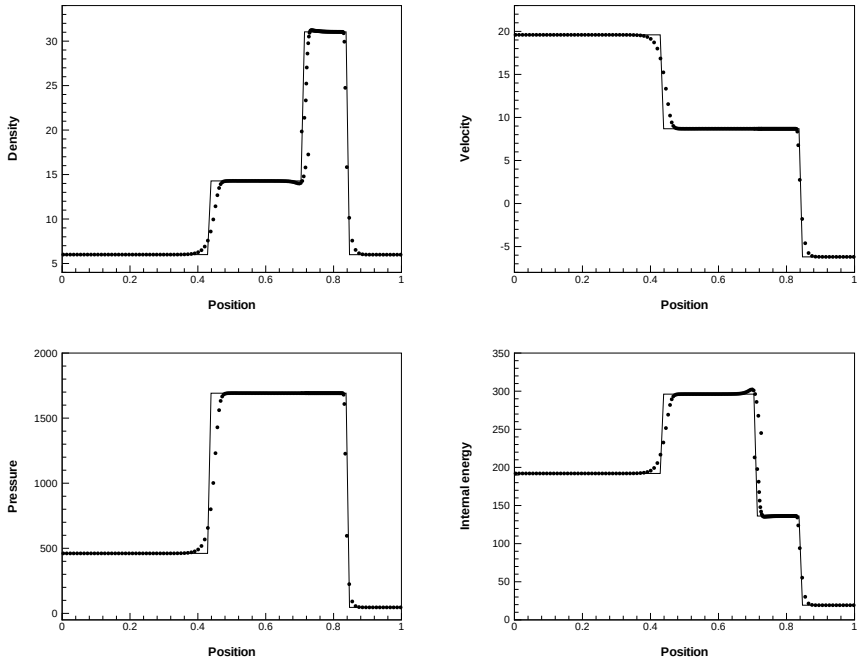

Figure 21: The Godunov-type SPH scheme with the modified Roe flux applied to test 4. Numerical (symbol) and exact (line) solutions are compared at the time 0.035 units.

method of Sigalotti *et al.* [21] produces spurious oscillations and it seems to be not conservative, because it computes wrong solution profiles in the star region. In fact, keeping a variable smoothing length is believed to be incompatible with the global conservation of the SPH method [2] and moreover it is not clear whether the variable smoothing length guarantees good consistency with the PDE [25]. The Godunov-type SPH scheme produces a jump within the contact wave, more evident using the Rusanov flux. Note that this is present only in the physical space (x,t) and not in the computational domain (ξ,t), because only in this domain the particles are moving. This phenomenon derives from an error in the numerical estimation of the integral (3.4), necessary to translate the solution profiles into the physical space (x,t). The algorithm based on (3.5) is of the second-order (Euler time integration). In future developments, a more accurate formulation of higher order can be chosen, so that the inter-penetration resulting in this test case can be solved. Nevertheless, the modified Roe flux produces once more the most accurate numerical results in comparison with the Rusanov flux and the Godunov flux.

4 Conclusion

In this paper, we have proposed alternative SPH approaches, stable without the Monaghan artificial viscosity term. They consist of the second-order SPH scheme, that mimics the classical Lax-Wendroff finite difference scheme, and the first-order Godunov type SPH scheme following Vila [25].

Both are linearly stable, as seen in Section 2. A von Neumann stability analysis has been carried out for the Lax-Wendroff type SPH scheme and the Godunov-type SPH scheme applied to the linear one-dimensional advection equation. For both we have obtained a range of Courant numbers, related to the ratio of mesh size and smoothing length, which assures linear stability.

The second-order Lax-Wendroff type SPH method is a linearly stable and less diffusive numerical scheme. Unfortunately it is not monotone. The Godunov-type SPH scheme is linearly stable *and* monotone, but it exhibits a large amount of numerical diffusion, especially for long-time evolution problems. In both methods, the classical artificial viscosity term of Monaghan, which usually needs the careful calibration of several parameters, has been completely removed and has been replaced by an intrinsic numerical viscosity that needs no (or at most one) parameter to be fixed.

Subsequently, the problem of the consistency conditions has been regarded. It is well-known that the classical SPH scheme does not always satisfy the consistency conditions. In this paper, a new approach for the Euler equations of compressible gas dynamics is proposed. It is always consistent for an initially uniform distribution of the elements. It consists of using Godunov-type SPH schemes in Lagrangian coordinates. In this approach, the positions of interpolation points are fixed during time evolution in Lagrangian coordinates (computational space) while they are moving in Eulerian coordinates (physical space). The scheme has been applied to some well-known test cases [22].

The numerical results are compared with the exact and numerical reference solutions. We can assert that the Godunov-type SPH scheme in Lagrangian coordinates provides an improvement in the accuracy. The scheme is still able to handle large deformations of the computational domain without requiring any specific algorithm to rezone the mesh.

Future developments of the proposed Godunov-type SPH schemes in Lagrangian coordinates may concern the extension to multiple space dimensions and to free-surface flows as well as interactions between fluids and solids.

References

[1] D.S. Balsara, Von Neumann stability analysis of smoothed particle hydrodynamics – Suggestions for optimal algorithms, J. Comput. Phys., 121 (1995), 357–372.
[2] G.V. Bicknell, The equations of the motion of particles in smoothed particle hydrodynamics, SIAM J. Sci. Stat. Comput., 12 (1991) 1198–1206.
[3] S.-H. Cha and A.P. Whitworth, Implementations and tests of Godunov-type particle hydrodynamics, Mon. Not. R. Astron. Soc., 340 (2003), 73–90.
[4] R. Courant and K.O. Friedrichs, Supersonic flow and shock waves. New York, Springer, 1976.
[5] R.A. Gingold and J.J. Monaghan, Smoothed particle hydrodynamics: theory and applications to non-spherical stars, Mon. Not. R. Astr. Soc, 181 (1977), 375–389.
[6] W.H. Hui, The unified coordinate system in computational fluid dynamics, Commun. Comput. Phys., 2 (2007), pp. 577–610.
[7] S.-I. Inutsuka, Reformulation of smoothed particle hydrodynamics with Riemann solver, J. Comput. Phys., 179 (2002), 238–267.
[8] S. Li and W.K. Liu, Meshfree and particle methods and their applications, Appl. Mech. Rev., 55 (2002), 1–34.
[9] M.B. Liu, G.R. Liu and K.Y. Lam, Constructing smoothing functions in smoothed particle hydrodynamics with applications, J. Comp. Appl. Math, 155 (2003), 263–284.
[10] W.K. Liu, S. Jun and Y.F. Zhang, Reproducing kernel particle methods, Int. J. Num. Meth. Engrng., 20 (1995), 1081–1106.
[11] L.B. Lucy, A numerical approach to the testing of fission hypothesis, Astronom. J., 82 (1977), 1013–1024.
[12] J.J. Monaghan, SPH meets the shocks of Noh. Monash University preprint, 1988.
[13] J.J. Monaghan, On the problem of penetration in particle methods, J. Comput. Phys., 82 (1989), 1–15.
[14] J.J. Monaghan, SPH without a tensile instability, J. Comput. Phys., 159 (2000) 2, 290–311.
[15] J.J. Monaghan and J.C. Lattanzio, A refined particle method for astrophysical problems, Astron. Astrophys., 149 (1985), 135–143.
[16] B.B. Moussa and J.P. Vila, Convergence of SPH Method for scalar nonlinear conservation laws, SIAM J. Numer. Anal., 37 (2000) 3, 863–887.
[17] C.D. Munz, On Godunov-type schemes for Lagrangian gas dynamics, SIAM J. Num. Anal., 31 (1994) 1, 17–42.
[18] A.N. Parshikov, S.A. Medin, I.I. Loukashenko and V.A. Milekhin, Improvements in SPH method by means of interparticle contact algorithm and analysis of perforation tests at moderate projectile velocities, Int. J. Impact Engng., 24 (2000), 779–796.

[19] N.J. Quinlan, M. Basa and M. Lastiwka, Truncation error in mesh-free particle methods, Int. J. Numer. Meth. Engng., 66 (2006), 2064–2085.
[20] M.X. Rodriguez-Paz and J. Bonet, A corrected smooth particle hydrodynamics method for the simulation of debris flows, Numer. Meth. Partial Diff. Eqns, 20 (2003), 140–163.
[21] L.Di G. Sigalotti, H. Lopez, A. Donoso, E. Sira and J. Klapp, A shock-capturing SPH scheme based on adaptive kernel estimation. J. Comput. Phys., 212 (2006), 124–149.
[22] E.F. Toro, Riemann Solvers and Numerical Methods for Fluid Dynamics: A Practical Introduction. 2nd. ed., Springer, 1999.
[23] B. Van Leer, Towards the ultimate conservative difference scheme, J. Comput. Phys., 32 (1979), 101–136.
[24] B. Van Leer, Upwind and high-resolution methods for compressible flow: From donor cell to residual-distribution schemes, Commun. Comput. Phys., 1 (2006), 192–206.
[25] J.P. Vila, On particle weighted methods and smooth particle hydrodynamics, Math. Models Methods Appl. Sci., 9 (1999) 2, 161–209.
[26] D.H. Wagner, Equivalence of Euler and Lagrangian equations of gas dynamics for weak solutions, J. Differ. Equations, 68 (1987), 118–136.